JOURNAL OF MATERIALS SCIENCE 20 (1985) 3428–3438

Microstructure and properties of $MgO–ZnO_2–SiO_2$ alkali-free glass–ceramics

ZU-XIONG CHEN
East China Institute of Chemical Technology, Shanghai, People's Republic of China
P. W. McMILLAN†
Department of Physics, University of Warwick, Coventry, UK

The glass-forming region of the $MgO–ZnO–SiO_2$ system with small additions of Al_2O_3 has been explored. Based on it, two alkali-free glass–ceramics nucleated by TiO_2 were produced, possessing high thermal expansion coefficient, microhardness and electrical resistivity. Investigation of the properties and microstructure of these glass–ceramics by means of scanning electron microscopy and X-ray diffraction indicates that the proportions of willemite solid solution, enstatite solid solution, and α-cristobalite which were encountered mainly in the glass–ceramics dominates the variation in properties. The mismatch of thermal expansion coefficient between the crystalline phases and the residual glass phase plays an important role in changing the mechanical properties.

1. Introduction

As early as 1962, Benecki and Hummel [1] produced by means of a sintering process a material based on a willemite solid solution (ss) of composition $(0.65\,Zn,\ 0.35\,Mg)_2SiO_4$ with high thermal stability and resistance to wear. Investigation of the $MgO–ZnO–SiO_2$ system indicated that many extensive ranges of willemite and enstatite ss existed in this system [2]. The similarity of the ionic radii of Mg^{2+} and Zn^{2+} allows some replacement in either structure to form willemite ss $(Mg, Zn)_2SiO_4$ or enstatite ss $(Mg, Zn)SiO_3$. A diagram of isofracts of glass was given [2], together with a description of glass formation with lower than 40 wt % SiO_2 obtained by quenching. Later on, several papers were published on technology, and crystallizing properties [3], catalysts [4] and the nucleation process [5] for producing $MgO–ZnO–SiO_2$ glass–ceramics. The glass-forming range in the system with additions of Na_2O and Al_2O_3 was investigated [3]. It was described as a fairly expanded glass-forming region, whereas only a very limited ternary glass-forming range was found around 40 wt % SiO_2. The glass-forming range of compositions which are alkali-free has not been defined previously, and papers on the dependence of the properties of $MgO–ZnO–SiO_2$ glass–ceramics on the microstructure have not to our knowledge appeared.

One aim of the present work was to explore alkali-free $MgO–ZnO–SiO_2$ glass–ceramics with high electrical resistivity, medium to high thermal expansion coefficient, and good mechanical properties. A further objective was to investigate the dependence of their properties on microstructure and composition.

2. Experimental procedure

According to previous work [3] and the publications on enstatite-containing $MgO–Al_2O_3–SiO_2$ glass–ceramics and willemite-containing $ZnO–Al_2O_3–SiO_2$ glass–ceramics, it was clear that Al_2O_3 could be a valuable additive in order to form $MgO–ZnO–SiO_2$ glasses.

The glass-forming range of the $MgO–ZnO–SiO_2$ system with 5 wt % Al_2O_3 extra addition was determined by melting 50 g glass at 1450° C for 3 h in a platinum crucible, followed by casting

† The death of Professor Peter McMillan is sadly recorded.

0022–2461/85 $03.00 + .12

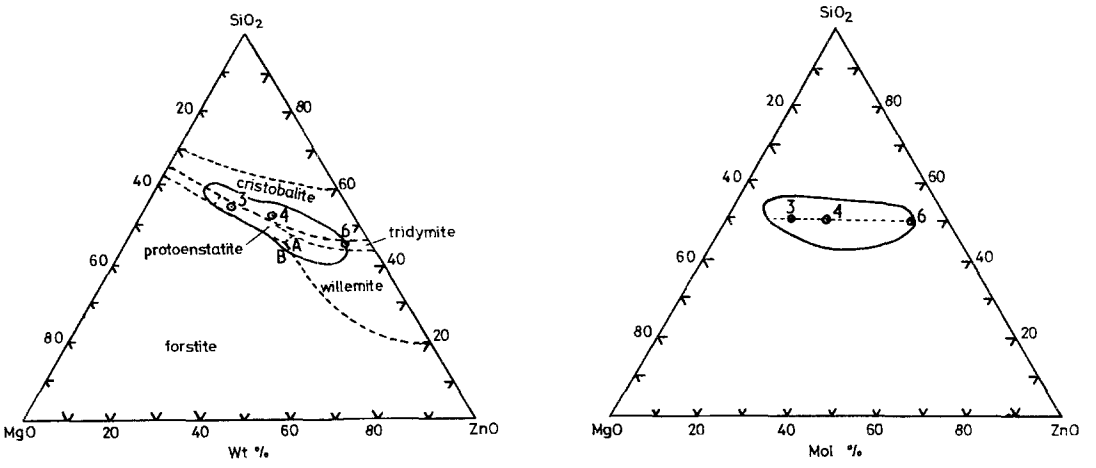

Figure 1 Glass-forming range for Mg–ZnO–SiO_2 system with 5 wt % Al_2O_3 additive.

it on a steel plate and pressing into a disc. The boundary of the glass-forming range was delineated by compositions which partially devitrified. In order to examine the crystallization in different compositions, specimens with the same molecular percentage of SiO_2 but with different MgO and ZnO substitutions (see Fig. 1 below) were chosen for heat treatment at 850, 880 and 910° C for 1 h. The compositions of glass–ceramics 1 and 2 are listed in Table I. Glass batches were mixed in a tumbling mixer for 4 h, followed by melting in a platinum crucible at 1520° C for 2 h. The melt was stirred once with an alumina rod during this period. It was poured into cold water and crushed into small pieces. The cullet was mixed and melted again at 1520° C, for 2 h. It was stirred once again. The forming process was completed by casting the melt on to a steel plate and pressing it into a disc about 2 to 3 mm thick, followed by annealing at 650° for 4 h. Glasses 1 and 2 were nucleated for 1 h at 680 and 725° C respectively, followed by heat treatment for 1 h at various temperatures between 800 and 1200° C, for investigation of the variation of microstructure and properties.

TABLE I Compositions of MgO–ZnO–SiO_2 glass–ceramics

Composition	Glass 1		Glass 2		Starting Material
	wt %	mol %	wt %	mol %	
SiO_2	55	51.39	54.84	54.94	Quartz
MgO	25	34.81	15.45	23.08	$MgCO_3$
ZnO	20	13.80	29.71	21.97	ZnO
Al_2O_3*	10	5.49	9.30	5.49	Al_2O_3
TiO_2*	5	3.53	5.84	4.40	TiO_2

*Extra component.

Differential thermal analysis (DTA) and differential scanning calorimetry (DSC) were used to determine the glass transition temperature T_g and the crystallizing temperature. X-ray diffraction and scanning electron microscopy (SEM) for specimens treated at various temperatures were recorded with a Philips 1380 diffractometer and a Cambridge Stereo 250 microscope respectively. Bulk samples were used in the X-ray diffraction tests. Polished specimens and back-scattered electron photography were found to be best for taking SEM images in the present work. The measurement of microhardness was carried out with a Vickers Microhardness Instrument M12a. An average of ten determinations was used in the calculation of Knoop hardness for one sample.

3. Results and discussion

3.1. Glass formation and devitrification

The glass-forming range of the MgO–ZnO–SiO_2 system with 5 wt % extra Al_2O_3 is illustrated in Fig. 1. Comparing with the phase diagram of the system without additives, the glass-forming range encloses two eutectics (Points *A* and *B*) and extends across the willemite, proto-enstatite, tridymite and cristobalite crystalline fields. Generally, it coincides in shape and location with the glass-forming range of compositions with additions of alkali metal oxides and Al_2O_3, but is slightly smaller. A very limited ternary glass-forming range along the 40 wt % SiO_2 line has been reported [3] but this was not confirmed in the present work. Alumina crucibles were employed in the previous work to investigate the glass-forming range, and as a result the compositions produced undoubtedly contained alumina. It can be noted

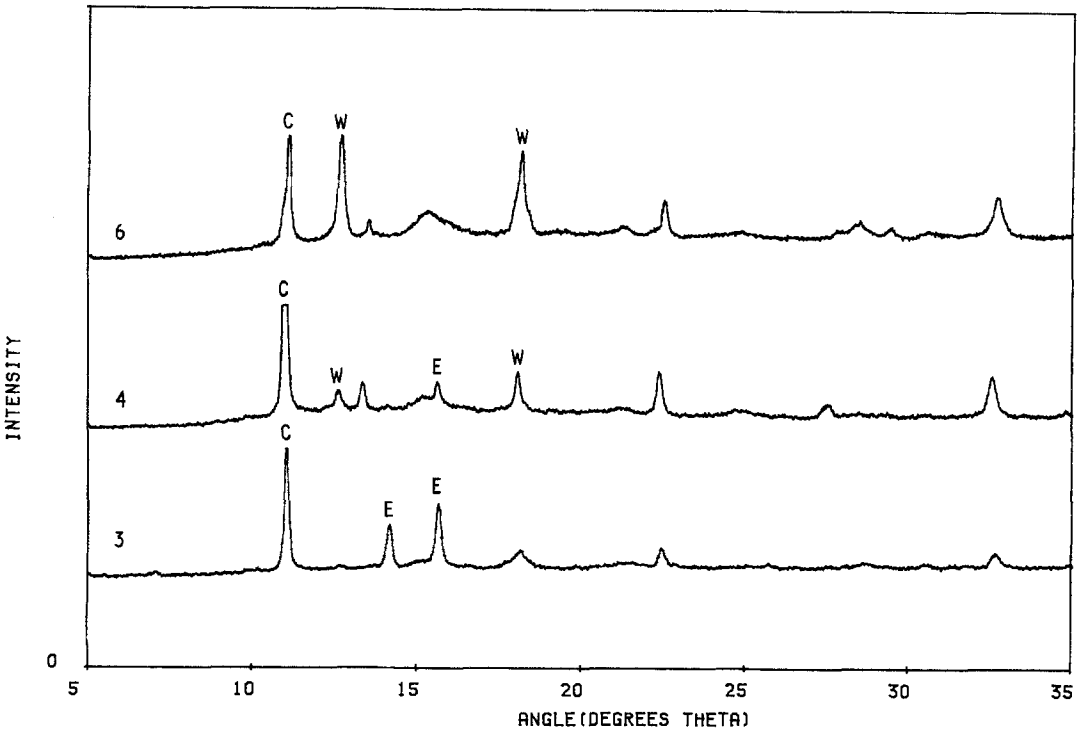

Figure 2 X-ray diffraction patterns for Glasses 3, 4 and 6 heat-treated at 910° C for 1 h; C = cristobalite, W = willemite ss, E = enstatite ss.

from Fig. 1b that the glass-forming range generally followed the line of 50 mol% SiO_2.

Aluminium oxide significantly influenced glass formation in the MgO–ZnO–SiO_2 system. With this addition, the glass-forming range could be extended widely. In the range of 5 to 10 wt% additional Al_2O_3, the higher the alumina content the larger the glass-forming range. For example, the composition 55 SiO_2:15 MgO:30 ZnO (wt%) with the addition of 5% Al_2O_3 could not form a transparent glass, whereas the same basic composition containing an additional 8.5 wt% Al_2O_3 could give a largely clear glass. Glass without any addition of Al_2O_3, even at the eutectic composition, could not be produced in a fully transparent form. However, glass having the eutectic composition but containing an additional 5% Al_2O_3 could be produced on a scale of hundreds of grams without any sign of devitrification.

It can be observed from the phase diagrams of the MgO–Al_2O_3–SiO_2 and ZnO–Al_2O_3–SiO_2 systems [6] that along the MgO–SiO_2 binary side the addition of Al_2O_3 always decreases the liquidus temperature when the SiO_2 content exceeds, i.e. when the SiO_2 content is higher than that of $MgSiO_3$. In addition, along the ZnO–SiO_2 binary side the introduction of Al_2O_3 also causes a lowering of the liquidus temperature when the content of SiO_2 exceeds 20%, but the addition of Al_2O_3 in amounts greater than about 10% increases the liquidus temperature again. Hence in compositions having SiO_2 contents above the $MgSiO_3$–$ZnSiO_4$ line in the ternary MgO–ZnO–SiO_2 system, the addition of Al_2O_3 will effectively decrease the liquidus temperature and improve glass formation.

Three glass compositions with the same silica content but with increasing ratios of zinc oxide to magnesium oxide were chosen for heat treatment (Fig. 1, Points 3, 4 and 6). It was found that the crystalline phases in Glass 3 heat-treated at 910° C for 1 h were α-crystobalite and enstatite ss, whereas Glasses 4 and 6 treated on same schedule as Glass 3 crystallized to give α-crystobalite, enstatite and willemite ss and α-cristobalite and willemite s.s. respectively (Fig. 2).

The compositions of Glasses 3, 4 and 6 lie in the enstatite, cristobalite and tridymite phase fields respectively (Fig. 1). Generally, their crystallizing paths coincide with the phase diagram, except that no tridymite was found in Glass 6. The proportion of α-cristobalite in the crystallizing

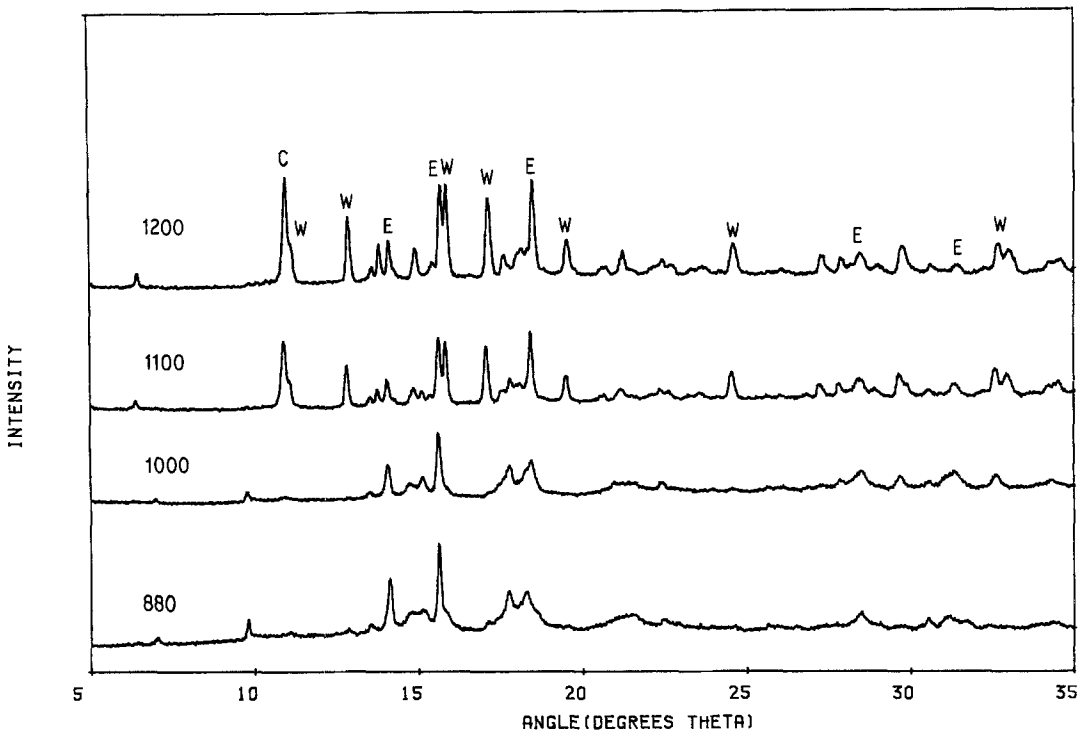

Figure 3 X-ray diffraction patterns for Glass 2 heat-treated at various temperatures; C = cristobalite, W = willemite ss, E = enstatite ss.

phases increases as follows: Glass 4 > Glass 3 > Glass 6. Enstatite ss and willemite ss were the major phases formed in Glasses 3 and 6, whereas α-cristobalite was the major phase formed in Glass 4 and showed fine crystalline structure.

Comparing with $MgO–ZnO–SiO_2$ + 3% Al_2O_3 + 3% Na_2O [3], the main difference on crystallization was the appearance of α-cristobalite in the compositions of high MgO. The similarity between the two systems is the relation of crystalline phases to the ZnO/MgO ratio, e.g. enstatite appears in compositions with high MgO content, whereas willemite appears in high ZnO compositions.

3.2. Crystallization processes and variation of microstructure for glass–ceramics nucleated by TiO_2

From X-ray diffraction analysis (Figs. 3 and 4) the crystallization processes for $MgO–ZnO–SiO_2$ glasses nucleated with TiO_2 were characterized by two stages.

For glasses 1 and 2, which are located in the enstatite and the cristobalite crystalline fields respectively, the first crystalline phase to appear was enstatite ss. Above 1000° C, α-cristobalite and willemite as emerged in Glass 2. With increase of temperature, the proportion of the three crystalline phases in Glass 2 varied with increase of the willemite and α-cristobalite contents (Fig. 3). However, the crystallization process of Glass 1 above 1000° C as indicated in Fig. 4 comprized the growth of enstatite ss and a small amount of α-cristobalite (Fig. 4). The DTA curve of Glass 1 was characterized by two broad exothermal peaks at 843 and 975° C, and three endothermal peaks at 1211, 1228 and 1266° C, corresponding to the fusion of three crystalline phases (Fig. 5). As with Glass 1, the DTA of Glass 2 demonstrated three exotherms at 872, 907 and 1040° C and three corresponding endotherms at 1230, 1245 and 1255° C. The exothermal peaks at 843, 872, 975 and 1040° C may be attributed to the crystallization of enstatite and α-cristobalite in Glasses 1 and 2 respectively, whereas the exotherm at 907° C which appeared only on the DTA curve of Glass 2 may be attributed to the emergence of willemite ss.

SEM gave additional information concerning the crystallization process. The enstatite ss crystals with a size below 1 μm were spread uniformly throughout the glass matrix, as shown in the

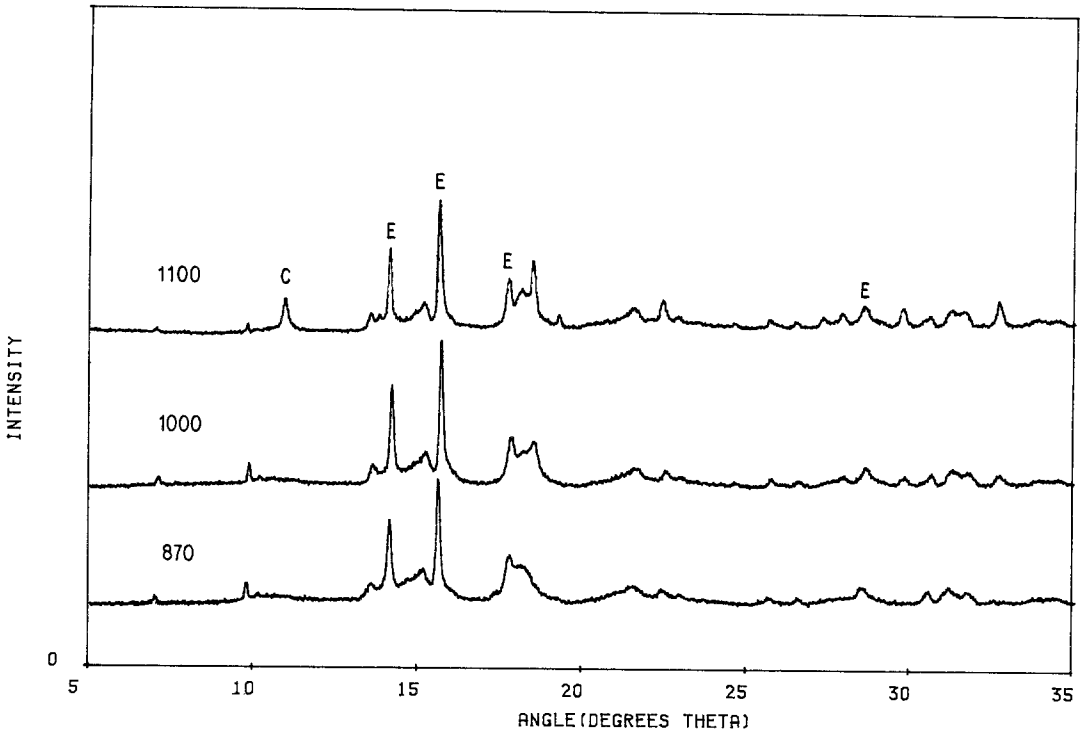

Figure 4 X-ray diffraction patterns for Glass 1, heat-treated at various temperatures; C = cristobalite, W = willemite ss, E = enstatite ss.

SEM picture for Glass 2 heat-treated at 880° C (Fig. 6a). After heat treatment above 900° C the microstructure of Glasses 1 and 2 divided into two phases, showing darker regions separated by a continuous and brighter phase (Figs. 6b and 7a). However, inside these two phases there still were very fine crystals, and no definite boundaries between these two phases could be observed (Figs. 6c and 7b). In contrast to Glass 1, there was a dramatic change of microstructure in Glass 2 after heat treatment at 1000° C for 1 h. New star-like crystals with a size of about 1 μm grew

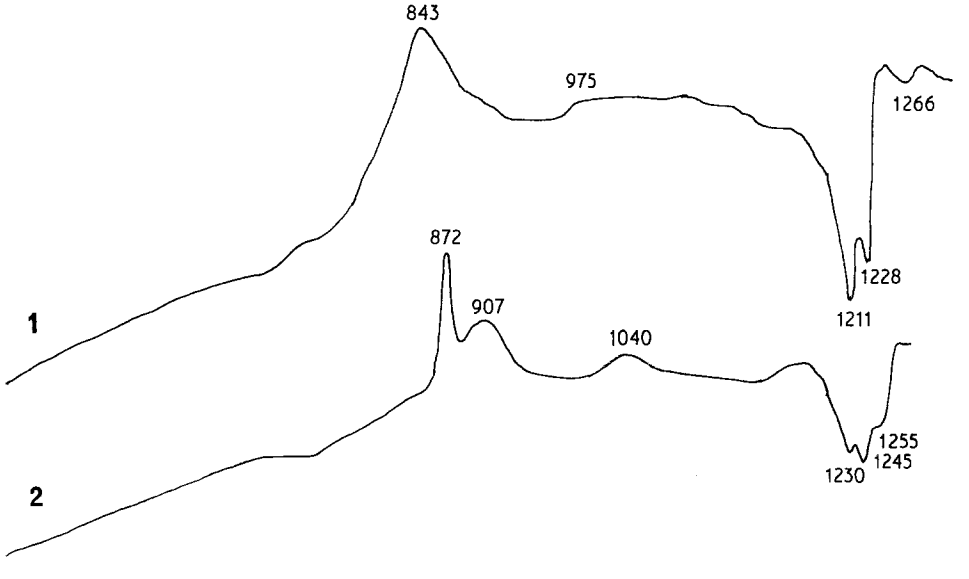

Figure 5 DTA curves for Glasses 1 and 2.

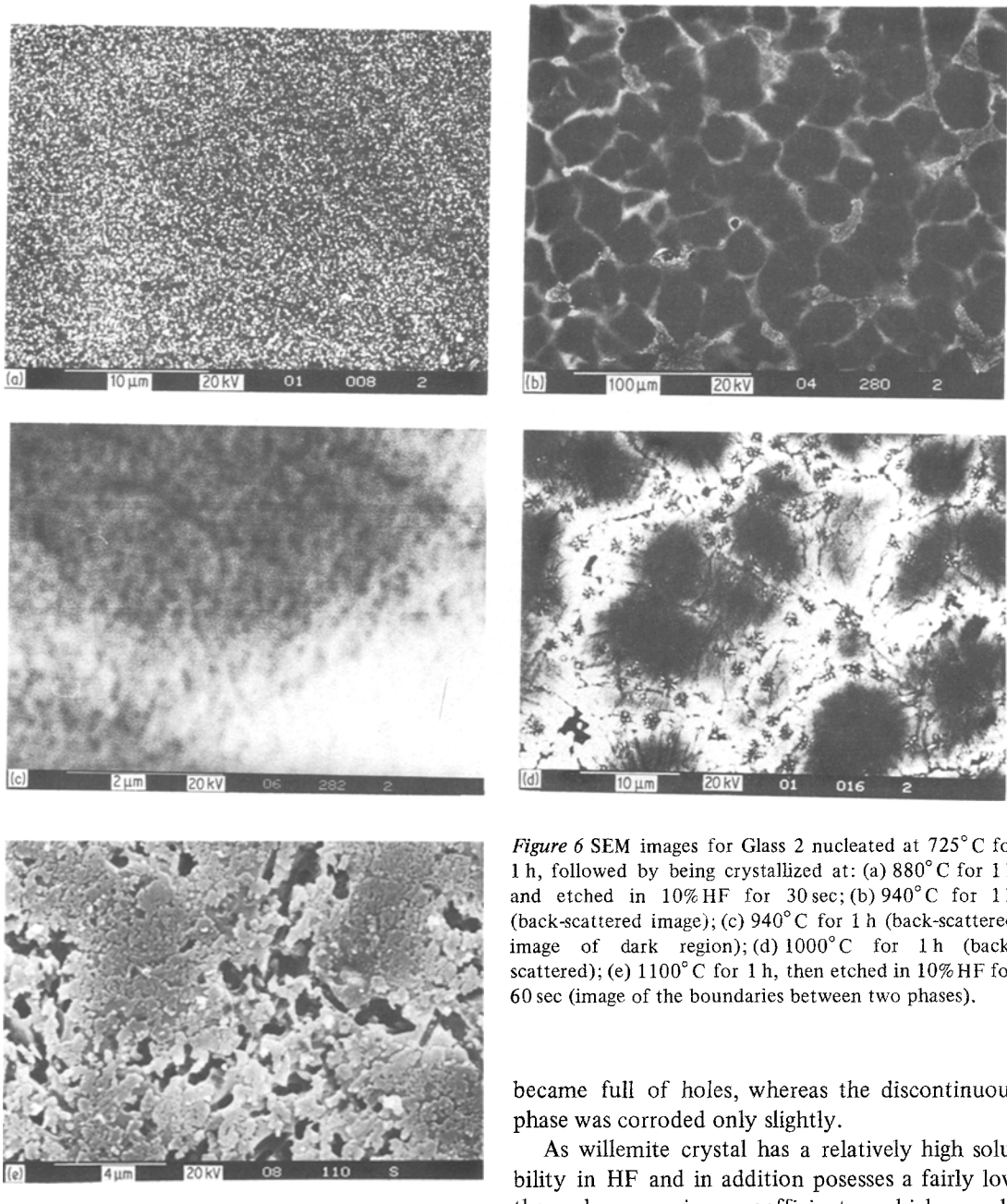

Figure 6 SEM images for Glass 2 nucleated at 725° C for 1 h, followed by being crystallized at: (a) 880° C for 1 h and etched in 10% HF for 30 sec; (b) 940° C for 1 h (back-scattered image); (c) 940° C for 1 h (back-scattered image of dark region); (d) 1000° C for 1 h (back-scattered); (e) 1100° C for 1 h, then etched in 10% HF for 60 sec (image of the boundaries between two phases).

in the continuous phase, most of them along the boundaries. The growth of these crystals yields microflaws in the material (Fig. 6d). This behaviour could not be observed in Glass 1 along the boundaries between the two phases, even though some small pores which seem to form from the contraction of the phase could be seen (Fig. 7c). Glass 2 was heat treated at 1100° C for 1 h and then etched in 5% HF solution for 1 min. Due to its high selective solubility in HF solution, in the SEM picture (Fig. 6e) the continuous phase became full of holes, whereas the discontinuous phase was corroded only slightly.

As willemite crystal has a relatively high solubility in HF and in addition posesses a fairly low thermal expansion coefficient, which could most probably be responsible for microflaws along the boundary of these two phases, the continuous phase in the SEM picture could therefore be identified as a zinc-rich area from which the star-like willemite ss crystallized. This zinc-rich or willemite ss phase exists also in Glass 1, as shown by Figs 7a and c, but the amount of it was small or the size of the crystals was so fine that the thermal effect of crystallization did not appear on the DTA curve, and no willemite peak emerged on the X-ray diffraction pattern. However,

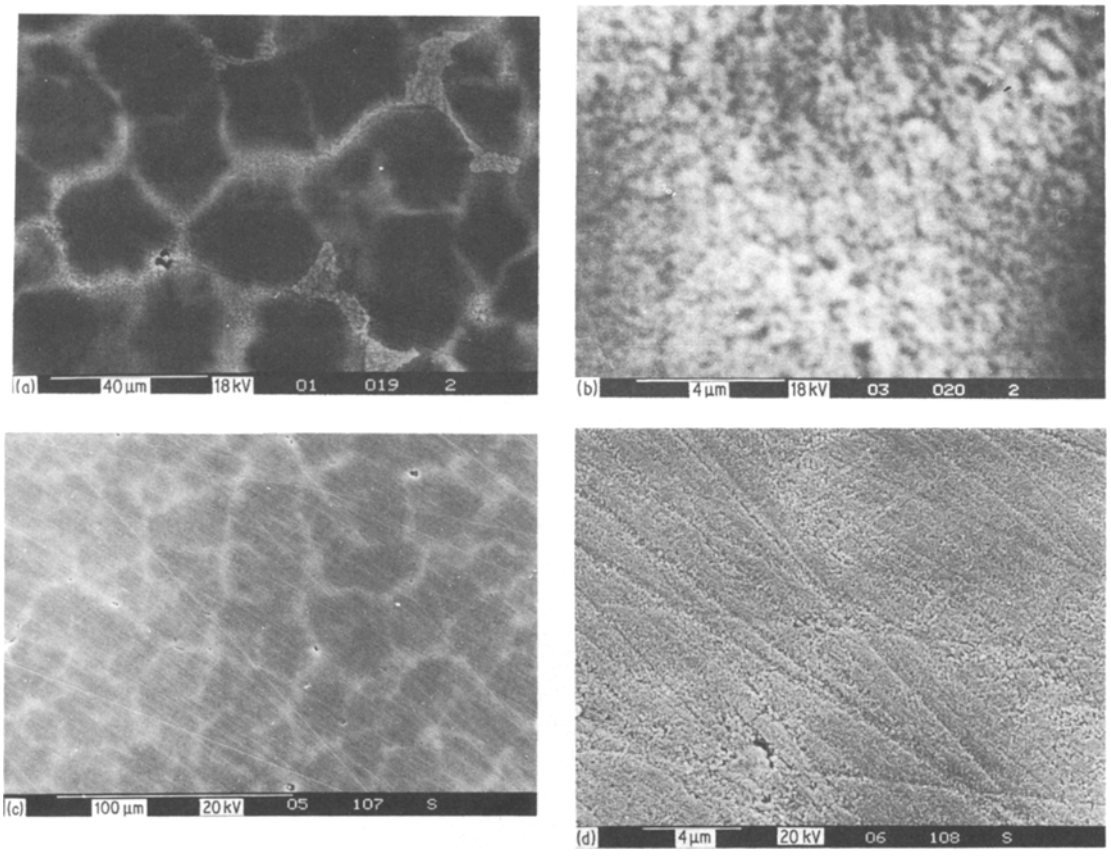

Figure 7 SEM image of Glass 1 nucleated at 725° C for 1 h, followed by being crystallized at: (a) 900° C for 1 h (back-scattered image); (b) 900° C for 1 h (back-scattered image of the dark area); (c) 1100° C for 1 h; (d) 1100° C for 1 h (image of the boundaries between two phases).

three fusion endotherms on the DTA curve of Glass 1 confirmed the existence of the phase.

To summarize, in $MgO–ZnO–SiO_2$ glasses with the catalyst TiO_2, containing ZnO but not as a dominant component, enstatite ss crystallizes first followed by its aggregation to form an MgO-rich phase separated by a ZnO-rich continuous phase. As the content of zinc oxide becomes fairly high, the willemite ss will grow up in the zinc-rich phase with an increase of the heat treatment temperature, and this will cause microflaws in the glass–ceramic due to the mismatch of thermal expansion coefficient with that of the residual glass phase.

3.3. Physical properties

3.3.1. Thermal expansion coefficient

The variation of thermal expansion coefficient against the temperature of heat-treatment is shown in Fig. 8. It can be observed that the variation of thermal expansion coefficient was characterized by a "stepped" curve. It indicates a close relation to the crystallization process in Glasses 1 and 2 (Fig. 8). Due to its fairly high thermal expansion coefficient (90×10^{-7} at 20 to 400° C, calculated from [7]) the crystallization of the enstatite ss yields a marked increase in thermal expansion for Glasses 1 and 2 heat treated at 900° C, i.e. twice the thermal expansion coefficients of their parent glasses. After heat treatment above 900° C, the willemite ss aggregated in the form of a continuous phase shown in the SEM photograph. Its low thermal expansion coefficient (16×10^{-7} at 20 to 400° C, calculated from [8]) compensated for the increase of thermal expansion due to crystallization of the enstatite ss, so that the net increase of thermal expansion coefficient became negligible; this formed the first step on the curve of thermal expansion coefficient against heat-treatment temperature curve (the α–T curve) for Glasses 1 and 2 (Fig. 8).

The crystallization of the willemite ss exhausted

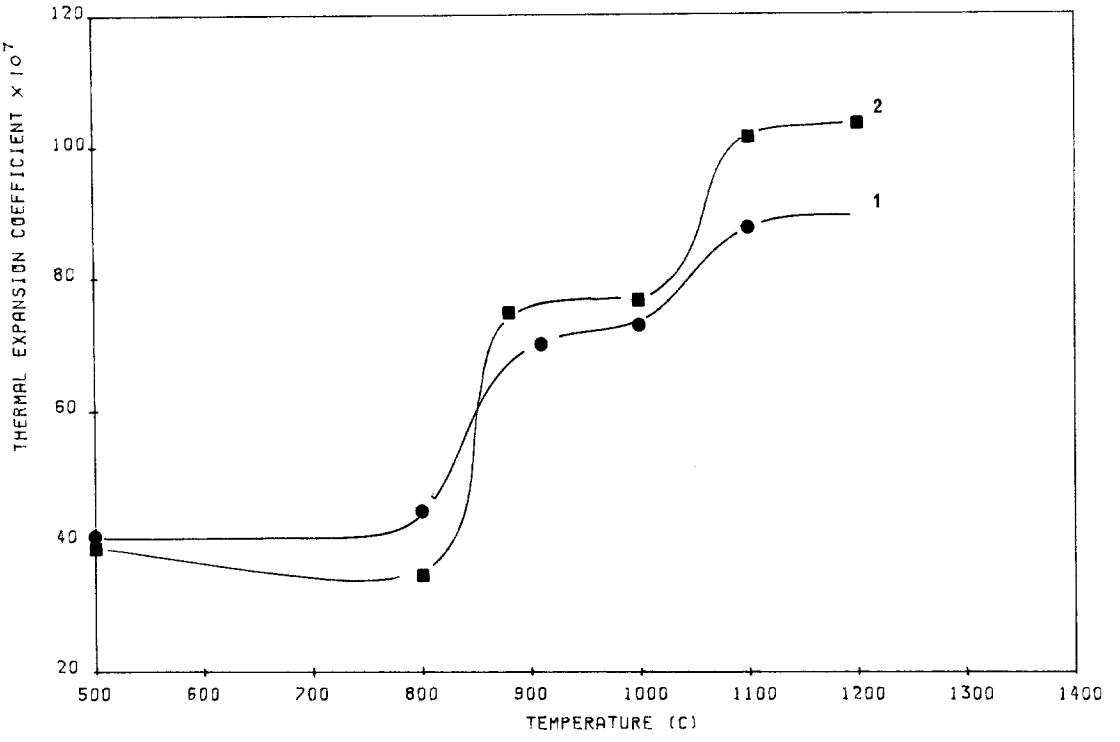

Figure 8 Variation of the thermal expanison coefficient of glass–ceramics heat-treated at various temperatures: • Glass 1, ▪ Glass 2.

the content of ZnO in the residual glass phase and induced the emergence of the α-cristobalite crystals, which have a high thermal expansion coefficient, increasing the thermal expansion coefficient of the material again. When the crystallization of α-cristobalite finished, the increase of thermal expansion coefficient stopped and a second step formed on the α–T curves. Similar α–T curves for Glasses 1 and 2 indicate similar crystallization procedures but different intensities. To form the enstatite ss $(Mg_xZn_y)SiO_3$ needs more SiO_2 than to form the orthosilicate willemite ss $(Mg_xZn_y)_2SiO_4$. This would be the most likely reason why a lesser amount of α-cristobalite crystallized from Glass 1, which contains more silica than Glass 2. This provided less increase of thermal expansion coefficient for Glass 1 treated above 1000° C than that for Glass 2 treated at same temperature.

3.3.2. Microhardness

The Knoop microhardness for Glasses 1 and 2 treated at various temperatures is shown in Fig. 9. A maximum at 950° C was present in the microhardness–temperature curve of Glass 2. For Glass 1, the microhardness increased markedly after 800° C heat treatment at 800° C, followed by a stable period in the range 900 to 1000° C, after which it increased to a maximum at 1100° C.

It may be observed that MgO–ZnO–SiO_2 glass–ceramics can be rather hard materials after heat treatment in an appropriate procedure. The main crystalline phases, willemite ss and enstatite ss, have hardness of about 5 to 6 on a Mohs scale, but Glasses 1 and 2 showed different characteristics for the variation of microhardness against heat-treatment temperature. From a microstructural point of view, the amount of willemite ss appearing in the glass–ceramics was the main difference between these two materials. Comparing with the analysis of microstructure in Section 3.2, this indicates that the crystallization of enstatite increases the microhardness of a glass–ceramic, whereas the emergence of willemite ss decreases it, or at least causes a retardation of the increase in hardness on the Knoop hardness–temperature curve (Fig. 9) between 900 and 1000° C.

Referring to the SEM photograph (Fig. 6d) a number of microflaws could be observed in

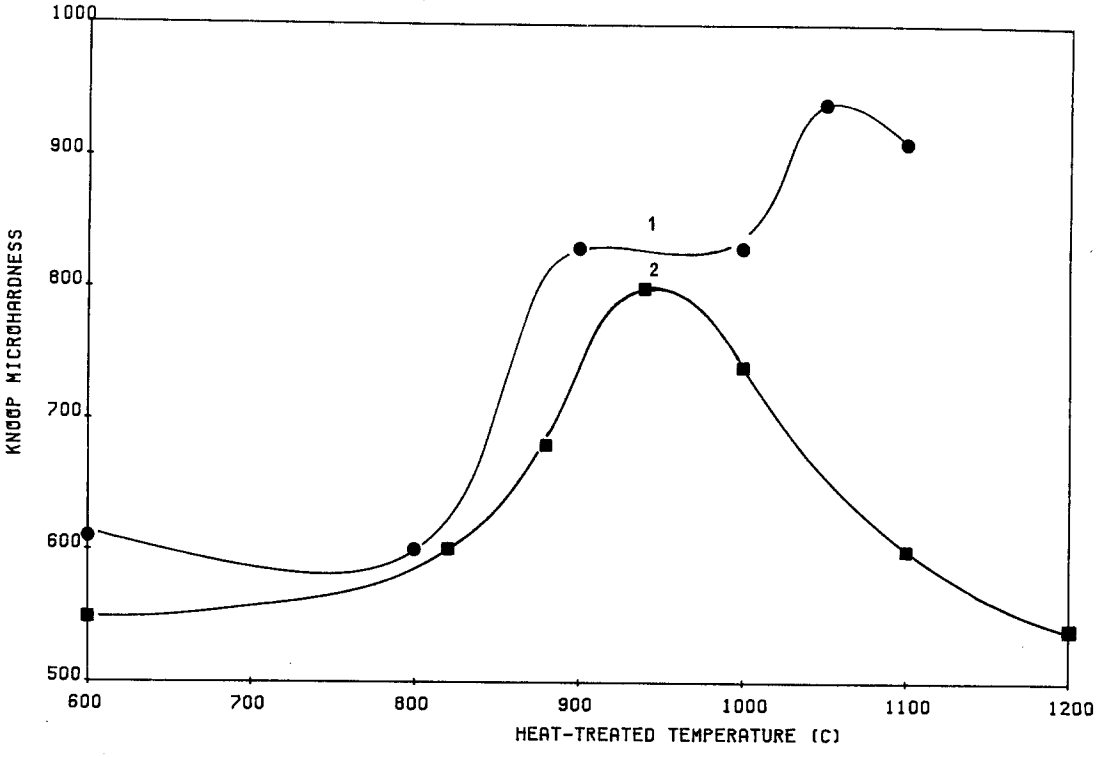

Figure 9 Variation of the microhardness for glass–ceramics heat-treated at various temperatures: • Glass 1, ▪ Glass 2.

Glass 2 treated above 950° C, which came from the mismatch of thermal expansion coefficients between the residual glass phase and the willemite crystals. The very low thermal expansion of the willemite crystals induced tensile stress in the glass matrix which reduced the microhardness of the material. The influence was so significant that for Glass 2 heat treated at 1200° C, for 1 h the microhardness could fall to that of its parent glass (Fig. 9).

However, in the case of low content of ZnO in Glass 1 the formation of willemite ss, which possessed very fine grain size and was present in a small amount that could not be identified by X-ray diffraction, did not have a considerable effect on the microhardness but retarded the increase in hardness. On the other hand, a mismatch of thermal expansion must occur also between the residual glass phase and the enstatite crystals, as the thermal expansion coefficients of the two original glasses are only about 40×10^{-7} and the crystallization of willemite and enstatite would not be able to increase the thermal expansion coefficient of the residual glass phase very much. Even so, the existence of a higher thermal expansion coefficient in the enstatite crystals than in the residual glass would only cause compressive stress in the residual glass, which would strengthen and harden the material. This could probably be the reason why the microhardness of glass–ceramics can be higher than those of all the crystalline phases encountered in the crystallization process. (A value of 7 on the Mohs scale would be comparable with a Knoop hardness of about 820.)

3.3.3. Electrical resistivity

As was expected, the electrical resistivities of the $MgO–ZnO–SiO_2$ glass–ceramics, which are alkali-free, are fairly high (Fig. 10). However, it was noticeable that the resistivities of the glass–ceramics were lower than those of their parent glasses, some even being decreased by four orders of magnitude (Fig. 10, Glass 1). At the same time the activation energies were also reduced and approached a similar level for Glasses 1 and 2 after crystallization (the activation energy of Glass 1 was $79.21 \pm 1.13\,kJ\,mol^{-1}$; for Glass 2 it was $72.35 \pm 0.5\,kJ\,mol^{-1}$). This may be attributed to there being the same mechanism of conductivity in the two glass–ceramics. As is well known, the temperature dependence of conductivity is

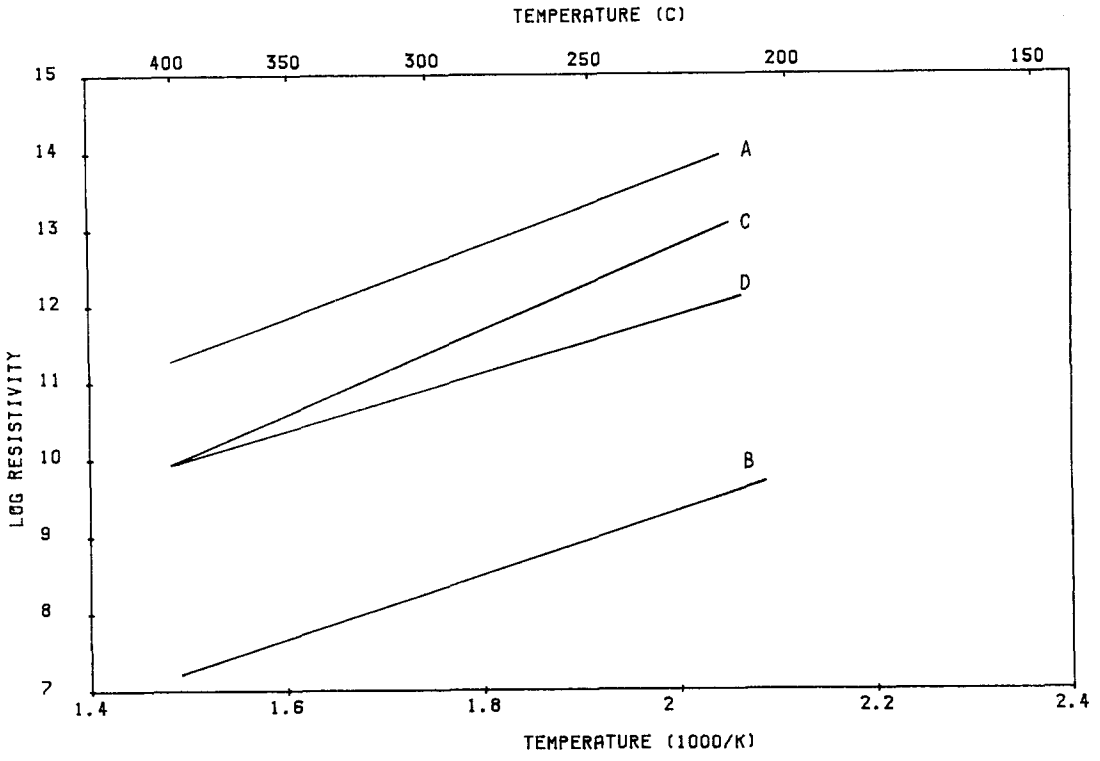

Figure 10 Resistivities against temperature for glass–ceramics: A = Glass 1; B = Glass–ceramic 1; C = Glass 2; D = Glass–ceramic 2.

given by

$$\sigma = \sigma_0 \exp(-E/KT)$$

where E is the activation energy of conduction and σ_0 is a pre-exponential term which can be expressed as $\sigma_0 = e^2\lambda^2 n\nu/2KT$; e is the electronic charge, λ the ionic jump distance, n the number of atoms per unit volume and ν the vibrational frequency of the ion in its well [8].

The activation energies for the two glass–ceramics are virtually identical, but the value of σ_0 for Glass 2 ($4.91 \times 10^{-5}\ \Omega^{-1}\,cm^{-1}$) is much smaller than that of Glass 1 ($8.4 \times 10^{-2}\ \Omega^{-1}\,cm^{-1}$). Since the crystallization processes for these two glasses are similar, consideration should be given to the alkali metal ions, which come from impurities in the raw materials, dominating the reduction in resistivity. This is the case where the alkali metal ions are incorporated into crystal phases, for instance in $ZnO–Al_2O_3–SiO_2$ glass–ceramics [6]; the effect of crystallization is to increase the concentration of alkali metal ions in the residual glass phase. This means that the electrical resistivity of $MgO–ZnO–SiO_2$ glass–ceramics would be sensitive to the purity of the starting materials.

4. Conclusion

The present work indicates that alkali-free glass–ceramics which possess high thermal expansion coefficient, hardness and electrical resistivity could be produced from the $MgO–ZnO–SiO_2$ system with small amounts of Al_2O_3 addition and with nucleation by TiO_2. The technological requirements for the production of these glass–ceramics are not very critical. The variation of their microstructure and properties is governed mainly by the appearance of willemite ss and enstatite ss. As the mismatch of thermal expansion coefficient between the crystalline phases and the residual glass phase produces strong effects on the mechanical properties, it would be necessary to take into account the cyrstallization process in the selection of compositions and heat treatment procedures to meet various applications.

References

1. W. T. BENECKI and F. A. HUMMEL, *J. Amer. Ceram. Soc.* **4** (1962) 290.
2. E. R. SEGNIT and A. E. HOLLAND, *ibid.* 8 (1965) 409.
3. E. N. ODELSKAYA and A. A. BRUBEL, "Glass, glass–ceramics, glass–ceramic materials" (in Russian)

3 (1973) 95.
4. A. A. BRUBEL and E. N. ODELSKAYA, *ibid.* 4 (1975) 163.
5. E. F. KARPOVICH, *ibid.* 9 (1980) 43.
6. E. M. LEVIN, H. F. McMURDIE and F. P. HALL, "Phase Diagrams for Ceramists", (American Ceramic Society, Columbus, Ohio, 1964).
7. J. F. SARVER and F. A. HUMMEL, *J. Amer. Ceram. Soc.* **4** (1962) 152.
8. P. W. McMILLAN, "Glass–Ceramics" (Academic Press, London, 1979).

Received 10 August
and accepted 13 September 1984